Environmental Science: Atmospheres

ROYAL SOCIETY OF CHEMISTRY

PAPER

View Article Online
View Journal | View Issue

Cite this: *Environ. Sci.: Atmos.*, 2025, **5**, 129

Estimating emissions of biogenic volatile organic compounds from urban green spaces and their contributions to secondary pollution†

Jinlong Ma,[a] Shuai Wang,[a] GuoChao Chen,[a] Shengqiang Zhu,[a] Peng Wang,[b] Jianmin Chen [a] and Hongliang Zhang *[acd]

The role of biogenic emissions in forming ozone (O_3) and secondary organic aerosol (SOA) is increasingly important with decreasing anthropogenic emissions in China. However, biogenic volatile organic compounds (BVOCs) from urban green spaces are often neglected mainly because available land cover datasets do not reflect the distribution and density of vegetation in urban areas. In this study, urban BVOC emissions in Beijing at 1 km spatial resolution are estimated based on Google Earth Engine and a high-resolution land cover dataset and then used for air quality simulation in the summer of 2017. The updated urban BVOC emissions show better agreement with observed isoprene emission fluxes than other inventories. Air quality simulation shows that the contribution of urban BVOCs to the maximum daily averaged 8 h O_3 in Beijing typically exceeds 5 ppb with the maximum value of 8 ppb. Although BVOC emissions are higher in rural areas than urban areas, their contributions to O_3 concentrations are lower in rural regions. In contrast, the mean concentrations of biogenic SOA (BSOA) in urban areas (1.44 μg m^{-3}) are 17% lower than in rural areas. Compared to other inventories, the average difference in BSOA concentrations in urban areas reached 0.18 μg m^{-3}, and the relative changes in ISOA, MSOA, and SSOA were 14.3%, 17.7%, and 32.6%, respectively. This study emphasizes the importance of considering BVOC emissions from urban green spaces in understanding urban atmospheric chemistry. The methodology used to update urban green spaces in this study is equally applicable to other cities.

Received 16th July 2024
Accepted 19th November 2024

DOI: 10.1039/d4ea00099d

rsc.li/esatmospheres

Environmental significance

Urban vegetation is an important part of the city and directly affects urban air quality. This study assesses the impact of vegetation emissions on urban air quality by using a 1 km spatial resolution of the biogenic volatile organic compound (BVOC) emission inventory. The findings show that ozone formed by BVOCs in Beijing urban areas typically exceeds 5 ppb with the maximum value of 8 ppb, which is higher than in rural areas. This study emphasizes the importance of considering BVOC emissions from urban green spaces in understanding urban atmospheric chemistry.

1 Introduction

Biogenic volatile organic compounds (BVOCs) are widely recognized as a group of critical chemical species emitted by the terrestrial ecosystem into the atmosphere,[1] and they account for 90% of VOC emissions globally.[2,3] BVOC emissions are mainly derived from plants and influence atmospheric composition due to their high reactivity.[3,4] They can undergo reactions with oxidants in the atmosphere, such as ozone (O_3), hydroxyl radicals (OH), and nitrate radicals (NO_3), leading to the formation of proxy radicals and other chemical species.[5]

BVOC emissions can be estimated with models, including the Model of Emissions of Gases and Aerosols from Nature (MEGAN), the European Biogenic Emission Model (BEM), the Global Biosphere Emissions and Interactions System (GloBEIS), *etc.*[6–8] While models provide a quantitative framework for studying BVOC emissions, bias exists between model estimates and observations,[9,10] and uncertainties in land data are one of the important contributors to this bias.[11,12] These uncertainties arise from vegetation classification, foliar biomass, vegetation distribution, emission rates of vegetation, *etc.*[13] Urban vegetation is a significant contributor to the underestimation of BVOCs. Although several land datasets with different spatial

[a]*Shanghai Key Laboratory of Atmospheric Particle Pollution and Prevention, Department of Environmental Science and Engineering, Fudan University, Shanghai, China. E-mail: zhanghl@fudan.edu.cn*

[b]*Department of Atmospheric and Oceanic Science, Fudan University, Shanghai 200438, China*

[c]*IRDR ICoE on Risk Interconnectivity and Governance on Weather/Climate Extremes Impact and Public Health, Fudan University, Shanghai, China*

[d]*Institute of Eco-Chongming (IEC), Shanghai 200062, China*

† Electronic supplementary information (ESI) available. See DOI: https://doi.org/10.1039/d4ea00099d

resolutions are available to use as model inputs,[14,15] it is still challenging to characterize vegetation in urban areas.[16]

Urban vegetation plays a significant role in shaping the urban environment and its BVOC emissions exhibit a strong correlation with the atmospheric conditions over urban areas.[17,18] Although the emission of BVOCs from urban areas is less than that from natural environments, BVOCs in cities can directly react with anthropogenic sources, particularly with nitrogen oxides (NO_x).[19] Studies also demonstrate that BVOCs impact surface O_3 by reacting with OH, particularly in urban areas dominated by VOC-limited regimes, where VOC emissions are constrained while NO_x is abundant.[18,20] Gao *et al.*[10] discovered that the contribution of BVOC emissions to O_3 production is twice as efficient in urban areas as in rural areas. Moreover, the higher urban temperature induced by urban heat islands will further increase the impact of BVOC emissions on O_3 in the urban atmosphere.[21] In addition to O_3, BVOC emissions emitted by urban vegetation play an important role in the formation of secondary organic aerosol (SOA) in urban areas and over one quarter of SOA concentrations were derived from biogenic SOA formed by BVOCs in most cities.[5,19,22]

Beijing, the capital city of China, is one of the biggest and most developed cities in China. Over the past 30 years, Beijing's urban area has expanded rapidly, increasing by 72.6% compared to 1992.[23,24] The continuous expansion of the urban area and the growth of people's demand for an ecological environment have led to a considerable increase in urban green space. Presently, urban green spaces of Beijing account for 49.77% of the urban area, an increase of 120% compared with 2002.[25] Expanding urban green spaces significantly elevates BVOC emissions and contributes to the formation of more secondary air pollutants.[26] These pollutants, in turn, are significant contributors to the air pollution in Beijing, especially the summer O_3.[27,28] In summer, high temperatures and intense solar radiation enhance photochemical reactions, resulting in ozone episodes in Beijing.[29–31] However, the lack of information on urban vegetation will affect the estimation of BVOCs and thus the prediction of air pollution.[16] Therefore, developing a high spatial resolution inventory of urban BVOC emissions in Beijing is vital.

In this study, a new method was introduced to determine the spatial distribution and area of urban vegetation. Using this method, an urban BVOC emission inventory in Beijing, called FROM-GLC10-U, was developed based on a 10 meter resolution land cover map (FROM-GLC10) and was evaluated with observations.[32] For comparison with FROM-GLC10-U, several BVOC emission inventories developed from commonly used land data were used. In addition, the BVOC emissions in the urban area of Beijing during the summertime and their contribution to air pollutants were determined.

2 Methodology

2.1 Data description

For estimating the BVOC emissions using the MEGAN model, it is necessary to determine the distribution and density of vegetation in land cover datasets.[13] Table S1† lists the satellite datasets used in this study. The Global LAnd Surface Satellite (GLASS) LAI product is developed based on the Moderate Resolution Imaging Spectroradiometer (MODIS) surface reflectance data, with the 500 meter spatial resolution and the 8-day temporal resolution.[33,34] A previous study indicated that the uncertainty of the GLASS LAI products is lower than that of the MOD15A2H product,[35] which is widely used, and therefore the GLASS is used as the LAI product in simulations.

Furthermore, four land cover datasets were used as the model inputs to estimate the BVOC emissions, including the Copernicus Climate Change (C3S) land cover product,[36] the MODIS MCD12Q1 land cover product,[37] the CGLS land cover product,[38] and the FROM-GLC10 product.[32] The spatial resolutions of these four land cover satellite products are 300, 500, 100, and 10 m, respectively. The FROM-GLC10 land cover images were developed based on FROM-GLC30, using 10 meter resolution Sentinel-2 images as well as Google Earth Engine. Compared to FROM-GLC30 and CGLS, FROM-GLC10 offers higher spatial resolution, allowing for better determination of various vegetation types and their distributions.[32,39] Therefore, FROM-GLC10 was selected as the base map for developing the new urban green map. Since FROM-GLC10 is only available for 2017, the base year for these products is 2017. Before being input to the model, the land cover data and the LAI data were pre-processed to the plant function types (PFTs) and the leaf area index of vegetation-covered surfaces (LAIv).[7] A detailed description of the pre-processed method of land data was described in Ma *et al.*[15] and Wang *et al.*[14] In addition, FROM-GLC10 has a generalized land type classification, considering only forest, grassland, cropland, *etc.*, and thus the vegetation types for FROM-GLC10 were first reassigned to match that of the MCD12Q1 product as described in Ma *et al.*[16] before being pre-processed into PFTs.

Vegetations were grouped into five major land cover types: needleleaf trees, broadleaf trees, shrubs, grass, and crops, based on PFTs used in the MEGAN model. The data on the tree and the shrub areas in Beijing were from the Beijing Municipal Forestry and Parks Bureau (BJ-MFPB) (available at **https://yllhj.beijing.gov.cn/zwgk/tjxx/**, last access: 10 January 2024), and the ratio between conifers and broadleaf trees were obtained to the data from the 7th national forest resource inventory.[40] In addition to tree and shrub areas, the areas of the grass and the crop were also collected, which is from the Beijing Statistical Yearbook (available at **https://tjj.beijing.gov.cn/tjsj_31433/**, last access: 12 January 2024). The total area of vegetation is similar for all four land cover products, but all are lower than the official data. The FROM-GLC10 dataset shows the highest area in broadleaf trees and the lowest area in conifers. This is because all forest types are uniformly categorized as forests in the FROM-GLC10 dataset, and according to the allocation rules described in Ma *et al.*,[16] if the grid in the FROM-GLC10 dataset was classified as a "forest" and the corresponding grid in the MCD12Q1 dataset is a conifer, that grid in the FROM-GLC10 dataset is assigned as a conifer. However, if the corresponding grid in the MCD12Q1 dataset is not a tree, the "forest" is categorized as the "broadleaf tree" in the FROM-GLC10 dataset.

Consequently, the relatively smaller area of conifer in the FROM-GLC10 dataset can be attributed to the smaller area of conifer in the MCD12Q1 dataset.

Isoprene flux was measured hourly in June 2017 (up to the 25th) using a proton transfer reaction-time-of-flight mass spectrometer (PTR-ToF-MS) at the Institute of Atmospheric Physics (IAP) in the urban central of Beijing with a height of 102 m (39.97°N, 116.37°E).[9] The concentrations of isoprene were measured in the same place and the same period using a dual-channel gas chromatograph with flame ionization detection (DC-GC-FID).[41]

2.2 Determination of urban green spaces

To identify the urban green spaces, the initial step is to determine the urban areas. This was achieved using the 'urban and built-up land' classification in the MCD12Q1 dataset as the basis for identifying urban areas. The boundaries of these identified urban areas were then projected onto other land cover datasets to ensure consistency and accuracy. Vegetation within the urban boundaries is recognized as the urban green space, as shown in Fig. 1. In the MCD12Q1 dataset, the coverage of urban green spaces is relatively lower compared to other datasets, particularly in the urban center, where vegetation cover is reported to be zero. The FROM-GLC10 dataset, on the other hand, indicates a relatively high percentage of urban green spaces, with vegetation cover exceeding 30% in most urban areas. Despite the higher spatial resolution and urban tree coverage in the CGLS dataset compared to the C3S dataset (Table S3†), the proportion of urban green space in the CGLS dataset is lower than that in the C3S dataset (Table S4†). This discrepancy is likely due to the underestimation of grass areas in urban settings. Additionally, while the FROM-GLC10 dataset reports a higher total area of urban green spaces than official data, the area of urban trees it identifies is only half of that reported in the official data. Generally, these land cover datasets all underestimate the area of urban trees.

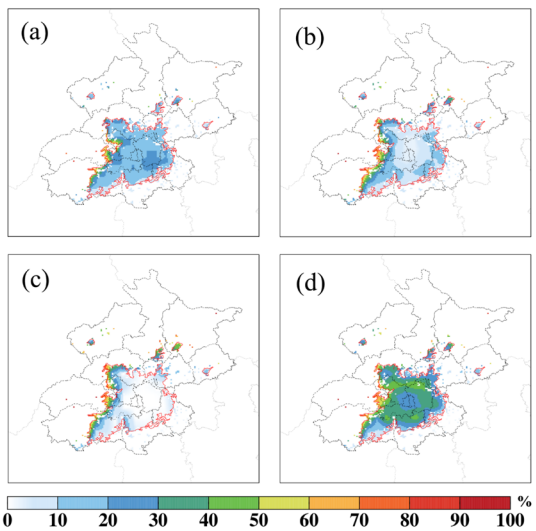

Fig. 1 Fractions of urban green spaces in Beijing from different land cover datasets ((a) C3S, (b) CGLS, (c) MCD12Q1, and (d) FROM-GLC10); the red line is the urban boundary. Percentage of vegetation in Beijing rural areas is not shown.

Subsequently, based on the urban boundaries, urban green spaces within the boundaries were identified through the high-resolution historical satellite images from Google Earth Pro and added to the PFT map converted by FROM-GLC10 to create the new PFT map. Google Earth Pro provides publicly available historical satellite imagery with a top-down perspective and allows users to zoom in and out of the imagery to show detailed features such as park trees, street trees, and residential trees. The detailed procedure for determining urban green spaces is shown below and Fig. 2 shows the work frame.

First, lines (named "polygons" in Google Earth Pro) are used to determine the boundary of urban green spaces and then marks are added to record the latitude and longitude of the polygon. After identifying all urban green spaces, save the file as a ".kmz" file and import it into ArcGIS to calculate the area of each polygon. Second, based on the domain in the model setup, the coordinate information for each polygon is converted from latitude and longitude to grid coordinates, representing the position of each polygon in the simulation region. Their areas are summed up if the polygons belong to the same grid. It should be noted that detailed information on the tree type is hard to recognize using this method. Therefore, the ratio of the needleleaf tree and the broadleaf tree within the urban area is also obtained from the 7th National Forest Resource Inventory.[40] Last, the area of each vegetation type within a grid was converted to a fraction based on the area of the grid and then allocated to the same grid coordinates as that in the model domain to generate a new PFT map, which is named FROM-GLC10-U. Fig. 2 shows that the urban green fraction of the FROM-GLC10-U dataset exceeds 10% in most areas and reaches up to 30% in Chaoyang and Haidian Districts. Although the urban green spaces in the FROM-GLC10 dataset are higher than that in the FROM-GLC10-U dataset, the areas of urban trees are lower than in the FROM-GLC10-U dataset (Tables S3 and S4†). In addition to the urban green spaces, the vegetation distributed outside the urban area in FROM-GLC10-U is adjusted based on the official data and the vegetation distribution in the FROM-GLC10 dataset, while the vegetation beyond the Beijing areas remains the same as in the FROM-GLC10 dataset.

2.3 Model description and application

The Community Multiscale Air Quality (CMAQ) model (v5.0.1), developed by the United States Environmental Protection Agency (US EPA), was configured to predict the air quality in this study.[42] The updated Statewide Air Pollution Research Center-11 (SAPRC-11) gas phase mechanism, which represents chemical reactions between atmospheric compositions in the gas phase, was applied in the model to determine SOA concentrations derived from isoprene, monoterpene and sesquiterpene, respectively.[43,44] A summary of the modified SAPRC-11 mechanism is presented below and a complete description is provided in Ying *et al.*[43] A more detailed isoprene oxidation scheme has been added to the modified SAPRC-11 mechanism, initially described by Lin *et al.*[45] and Xie *et al.*[46] This scheme considers

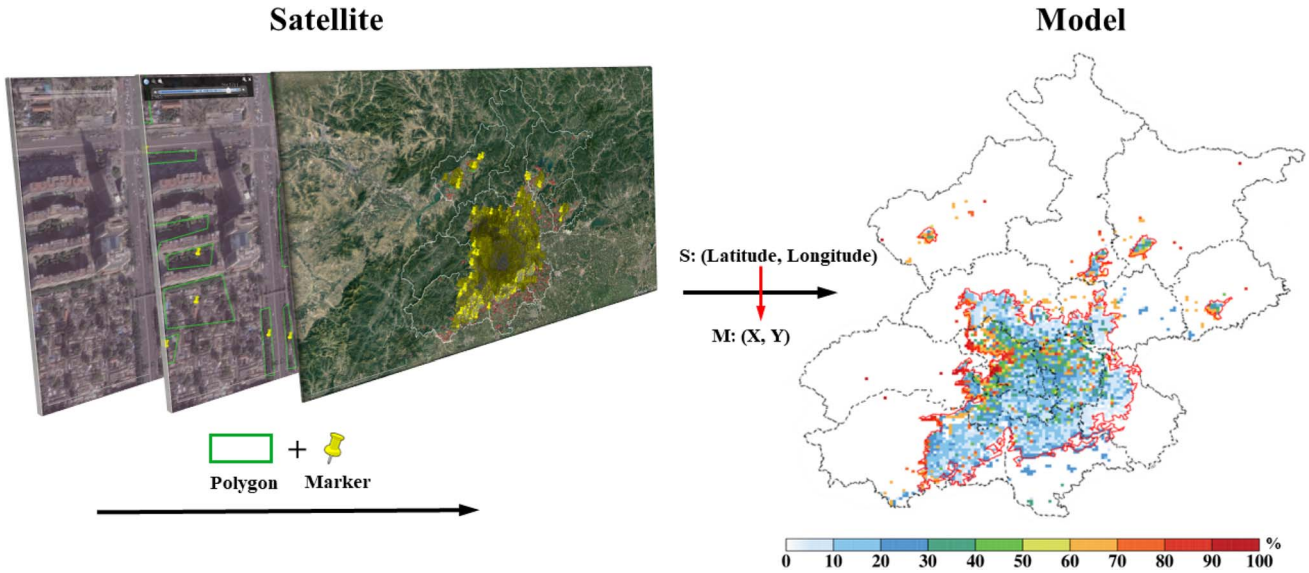

Fig. 2 Work frame of obtaining the urban vegetation region in the satellite image and inputting into the model. The right image is the fraction of urban green spaces in the FROM-GLC10-U dataset. Percentage of vegetation in Beijing rural areas is not shown.

the formation of IEPOX and MAE, suggested by Paulot *et al.*[47] and Lin *et al.*,[45] as well as more a detailed description of isoprene nitrate chemistry. Moreover, by using the method of tagging a precursor, the modified SAPRC-11 mechanism was further expanded to track six groups of precursors: (1) aromatics with OH reaction rates less than 2×10^4 ppm^{-1} min^{-1} (ARO1), (2) aromatics with OH reaction rates greater than 2×10^4 ppm^{-1} min^{-1} (ARO2), (3) isoprene (ISOP), (4) monoterpenes (TERP), (5) sesquiterpenes (SESQ), and (6) all other primary VOC precursors and direct emissions of GLY and MGLY.

The concentrations of O_3 and SOA and the source contribution from BVOC emissions for summer 2017 in Beijing were determined by implementing the modified CMAQ model. Higher resolution CTM studies can simulate more accurate meteorology, emissions and pollutant concentrations,[48–50] and therefore the model simulations were conducted in four nested domains with spatial resolutions of 36 km, 12 km, 4 km, and 1 km (Fig. S1 in the ESI†). The first 5 days of each simulation are used as spin-up and excluded from the analysis. The meteorological condition input for the CMAQ model was generated by utilizing the Weather Research and Forecasting (WRF) model v3.6.1 based on boundary and initial data from the National Centers for Environmental Prediction (NCEP) Final (FNL) Operational Model Global Tropospheric Analyses dataset. The WRF model used the same configuration as in previous studies and the physical options used in the model are listed in Table S2.†[15,51,52] The anthropogenic emissions of China in 2017 were adjusted based on the Multi-resolution Emission Inventory for China (MEIC) according to the description by Zheng *et al.*[53] and have been used in the previous study.[54] Meanwhile, the emissions from other countries were provided by the Emissions Database for Global Atmospheric Research (EDGAR) v4.3. MEGAN v2.1 was used to estimate biogenic emissions based on land datasets described in Section 2.1.

The simulation schemes are presented in Table 1. B1 to B5 use five different land cover datasets and the GLASS LAI dataset as the MEGANv2.1 inputs to estimate BVOC emissions from Beijing during the summer of 2017. It should be noted that the

Table 1 Simulation schemes with different land covers and leaf area indices (LAIs)

	BVOCs				
Case	Land cover	LAI	Meteorological condition	Air pollutants	Description
B1	C3S	GLASS	WRF	CMAQ	Simulated with the C3S dataset and the GLASS dataset
B2	CGLS				Simulated with the CGLS dataset and the GLASS dataset
B3	MCD12Q1				Simulated with the MCD12Q1 dataset and the GLASS dataset
B4	FROM-GLC10				Simulated with the FROM-GLC10 dataset and the GLASS dataset
B5	FROM-GLC10-U				Simulated with the FROM-GLC10-U dataset and the GLASS dataset

Table 2 Simulation designed to investigate the impact of biogenic emissions on Beijing air quality

Simulation	Description
B4	Full chemistry with anthropogenic and biogenic emissions with the FROM-GLC10 land cover dataset
B5	Same as B4 but with the biogenic emissions based on the FROM-GLC10-U land cover dataset
B4-NB	Same as B4 but without biogenic emissions in China
B4-BJNB	Same as B4 but without biogenic emissions in Beijing
B4-BJUNB	Same as B4 but without biogenic emissions in urban areas of Beijing

simulations are based on consistent meteorological data provided by the WRF model. With the exception of the BVOC emission, the other emission sources and settings were kept consistent in the simulation.

Since urban air quality can be improved by controlling the precursors of pollutants, and this approach only works for urban anthropogenic rather than urban biogenic emissions, it becomes important to understand how urban biogenic emissions contribute to air quality. Except for the CMAQ simulations with the biogenic inventory based on B4 and B5, three parallel CMAQ simulations with a horizontal resolution of 1 km are performed to investigate further impacts of BVOC emissions on O_3 and SOA in Beijing. The further sets of simulations are summarized in Table 2. Given that evaluation of isoprene emissions and concentrations simulated based on the FROM-GLC10 dataset is superior to other land cover datasets in this study, only BVOC emissions simulated with the FROM-GLC10 and FROM-GLC10-U datasets are used for parallel CMAQ simulations.

3 Results and discussion

3.1 Model performance

The WRF model simulations were evaluated by comparing the predicted temperature at 2 m (T2) above the surface, relative humidity (RH) at 2 m above the surface, wind speed (WS), and wind direction (WD) at 10 m above the surface with the observation data from National Climate Data Center (**ftp://ftp.ncdc.noaa.gov/pub/data/noaa/**). The equations of indicators are listed in Table S5† and validation results are shown in Table S6.† The model slightly overestimated the T2 with q mean bias (MB) value of 1.1 and a gross error (GE) value of 2.2, similar to previous studies.[14,55] The MB and GE value of WS met the benchmarks, while the prediction of RH was lower than the observation, which was comparable with those in previous studies.[55,56] Generally, the WRF model performed well, and predicted meteorological conditions are acceptable as inputs for the CMAQ model.

The CMAQ performance was validated using the observation data from the National Air Quality Monitoring Network (**http://www.cnemc.cn/**), as shown in Table S7.† The model predicted the O_3 concentrations in Beijing well, with a mean normalized bias (MNB) value of 0.11, which met the EPA benchmark.[57] Although the O_3 prediction is slightly higher than the observation, it is comparable to that in previous studies.[54,58] Meanwhile, the mean fractional bias (MFB) value and mean fractional error (MFE) value of $PM_{2.5}$ were within the criteria of 0.6 and 0.75, respectively. Overall, the CMAQ model accurately simulated the concentrations of air pollutants during the study periods.

3.2 BVOC emissions in Beijing

Fig. 3 shows the spatial variations of BVOC emissions in different cases in the Beijing region, including urban and rural areas. These cases show that BVOC emissions in Beijing are similarly distributed spatially and are mainly concentrated in the northern part of the city. The monoterpene and sesquiterpene emissions in most areas of Beijing are within the range of 0.1–0.5 mg m^{-2} h^{-1} and 0.02–0.06 mg m^{-2} h^{-1}, which are close to the results in Wang *et al.*[14] Previous studies have proven that trees and shrubs show high emission potentials in BVOC emissions, especially isoprene, while crops and grasses are generally considered to have low isoprene emissions.[13] Due to the high distribution of trees in the CGLS dataset, isoprene emissions from B2 are the highest among the three scenarios, which are 88.5% and 47.2% higher than that from the MCD12Q1 dataset and the C3S dataset, respectively (Table S8†). Besides the satellite datasets, Table S8† also presents the official statistics of vegetation areas in Beijing. Compared with the other two land cover datasets, the tree areas in the CGLS data are closer to the official data, indicating that the accuracy of the CGLS dataset in identifying trees is higher. Although the total vegetation area of these land cover data is comparable to that in Beijing, the vegetation area of the C3S dataset and the MCD12Q1 data is mainly distributed in grass and crops.

After adjusting the vegetation area in Beijing based on the land cover dataset FROM-GLC10 and the official data, the BVOC emissions in B5 are slightly higher than B4 in most areas but are lower than B4 to the west of Beijing. Although the official statistics on the area of broadleaf forests is less than the area in the FROM-GLC10 dataset, the two are comparable in terms of the area of trees, and the official statistics on shrublands are higher than in the FROM-GLC10 dataset, thus leading to the higher BVOC emissions in B5 than in B4 (Table S8†).

Typically, the vegetation density in rural areas is higher than in urban areas, leading to greater BVOC emissions in rural regions. However, the urban heat island effect increases VOC emissions in urban areas, especially for isoprene.[59] In the urban areas of Beijing, BVOC emissions are generally underestimated due to missing or insufficient information on vegetation coverage. As shown in Fig. 3, the MCD12Q1 dataset significantly underestimates the spatial distribution of urban green spaces in Beijing compared to other land cover datasets. The isoprene emissions in both B2 and B3 are below 0.4 mg m^{-2} h^{-1} in the

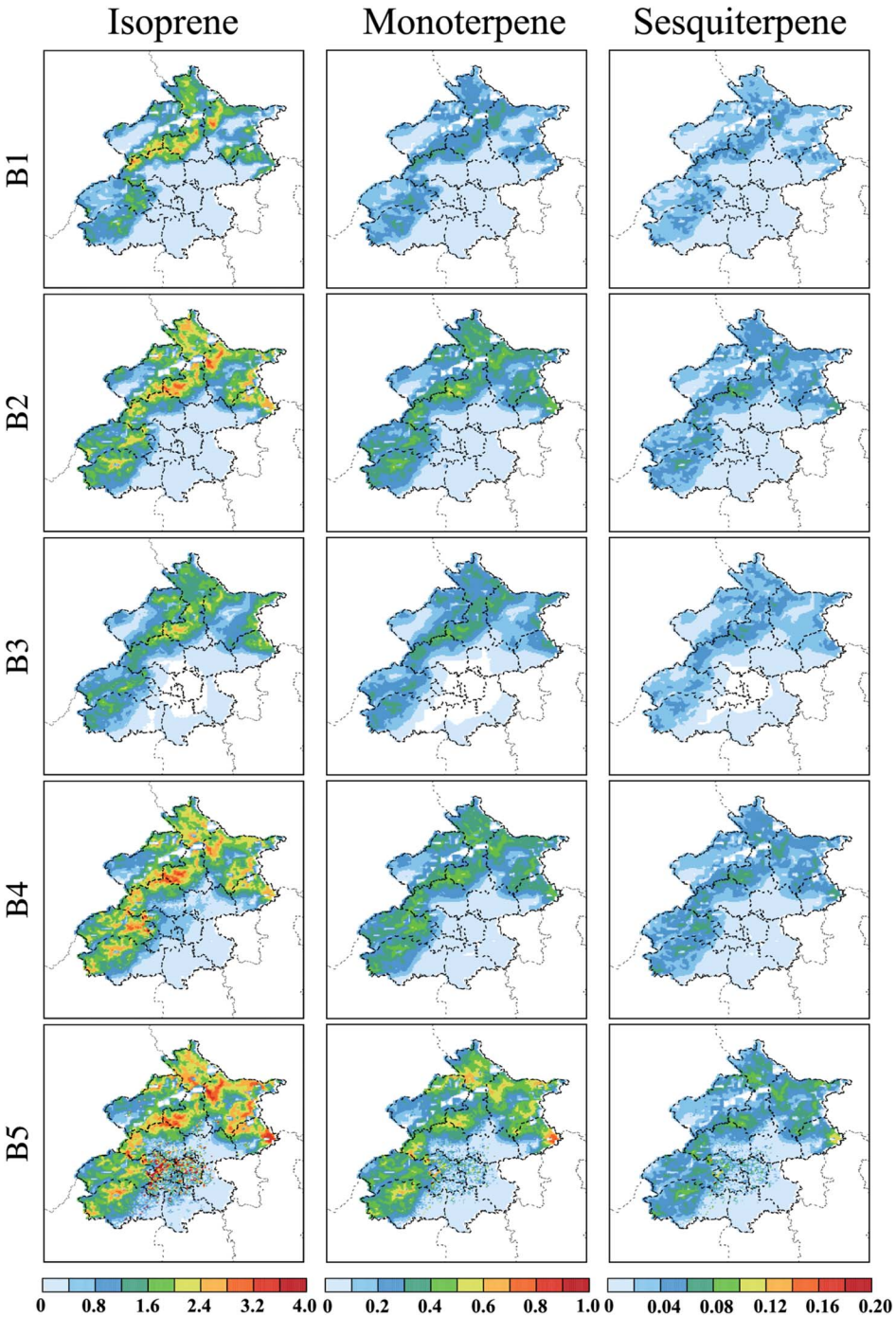

Fig. 3 Spatial distributions of main biogenic VOC species (isoprene, monoterpene and sesquiterpene) in Beijing (unit: mg m^{-2} h^{-1}).

urban areas of Beijing, while in B5, isoprene emissions exceed 0.8 mg m^{-2} h^{-1} (Fig. 3). Compared with B4, BVOC emissions from urban green spaces are higher in B5, especially in Chaoyang and Haidian districts. Here, the variation in isoprene emissions reaches up to 0.8 mg m^{-2} h^{-1}. This is due to the urban tree coverage in these two areas being updated through Google Earth, which increased vegetation cover by 434.6% and 90.7% (Table S3†). Although the areas of urban green spaces in B4 are higher than in 5, most of them are grass with low BVOC emission potentials (Table S4†).

BVOCs emitted by urban green spaces in Beijing are listed in Table 3. The total amount of BVOC emissions ranges from 2.40 to 13.40 Gg in the urban area of Beijing, with the highest in B5 and the lowest in B3. Isoprene emission is the dominant contributor to total BVOC emissions except B3, mainly due to the higher area fraction of crops in the MCD12Q1 product, which results in higher OVOC emissions. The total BVOC emissions in the urban areas based on the FROM-GLC10 dataset are 67.9%, 89.9% and 251.3% higher than those of the CGLS dataset, the C3S dataset, and the MCD12Q1 dataset primarily

Table 3 BVOC emissions (Gg) from urban green spaces in different cases in Beijing

	B1	B2	B3	B4	B5
Isoprene	1.86	2.33	0.98	4.94	9.05
Monoterpenes	0.26	0.44	0.13	0.45	1.16
Sesquiterpenes	0.06	0.08	0.03	0.09	0.21
OVOCs	2.27	2.17	1.27	2.94	2.97
Total	4.44	5.02	2.40	8.43	13.40

due to the higher urban tree covers. Interestingly, the area of urban trees increases with increasing spatial resolution of the land cover data, which is more in line with the official data (Table S5†), suggesting that improving spatial resolution of the land data is necessary. With updating based on official data, the FROM-GLC10-U dataset shows a lower urban green area than the FROM-GLC10 dataset, but more urban tree area in Beijing is identified through Google Earth in the FROM-GLC10-U dataset, resulting in 59% higher urban BVOC emissions for B5 than B4.

The urban BVOC emissions based on FROM-GLC10 and FROM-GLC10-U were compared with those in previous studies, as shown in Table 4. The estimated BVOC emissions in this study are generally within the ranges. The isoprene, monoterpene, and sesquiterpene emissions estimated based on FROM-GLC10 and the GLASS product were lower than those reported by Li *et al.*[60] This is likely because Li *et al.*[60] improved on the LAI dataset that previously underestimated the LAI in the urban green space. Ghirardo *et al.*[61] estimated urban BVOC emissions in Beijing and showed that emissions of BVOCs in urban areas doubled in the five years from 2005 to 2010 because of increased urban greening. The difference in BVOC emissions between this study and Ghirardo *et al.*[61] is also mainly induced by the increase in the urban green space, which was increased by 33.2% from 2010 to 2017 in Beijing, according to the data recorded in the BJ-MFPB. Ren *et al.*[26] used a field survey with 282 sample plots to obtain the city-level vegetation inventory, which is different from the inventory by marking vegetation positions based on satellite imagery. Although field surveys could accurately identify the type and area of vegetation within a given area, the limited scope of the study is likely to underestimate urban green space, leading to an underestimation of BVOC emissions.

3.3 Evaluation of isoprene emissions and concentrations

Fig. 4a compares observed (red points) and simulated (colored lines) isoprene emissions over urban Beijing during June 2017. Although there is only one observation point available during the study period, a large amount of observed isoprene emissions in this site came from the urban park due to the influence of summer wind. Therefore, the observations in this site can be used to represent the isoprene emissions emitted by the biogenic source.[9] Under the same meteorological conditions, all cases show a similar changing trend to the observations. Due to the differences in vegetation distributions, the quantity of isoprene emissions among scenarios varies B5 > B4 > B1 > B2. The mean fractional bias (MFB) and mean fractional error (MFE) between different cases and observations are listed in Table S9.† B3 shows no isoprene emissions in this location. The MFB and MFE values of B4 are −0.52 and 1.40, lower than those of B1 and B2. This indicates that B4 estimates BVOC emissions in Beijing urban areas more accurately than B1 and B2, although they all underestimate isoprene emissions. After updating the urban green spaces in Beijing using Google Earth, the isoprene emissions have nearly doubled in B5 compared to B4. Meanwhile, the simulation also shows a clear improvement and the MFB and the MFE values of B5 are reduced to −0.21 and 1.37, respectively. However, the simulation of B5 slightly overestimates the isoprene emissions. This is likely because some of the flux of isoprene may not be captured at the height of the 102 m, and this loss was not corrected in the study.[9]

In addition to the time series of isoprene emissions, the simulated and observed isoprene concentrations during June are evaluated and shown in Fig. S2.† The correction coefficient of B3 simulated with the MCD12Q1 dataset is almost zero due to the lack of information on urban green space in Beijing, resulting in zero isoprene emissions simulated at this site. Although the correction coefficients of B1 (0.59) and B4 (0.61) show a good correlation with the observations, the fitted line is sloped toward the axis on the side of the observations, indicating that the simulation underestimates the isoprene concentrations. By updating the urban tree information in Beijing using Google Earth Pro, the correction coefficient of isoprene concentrations between the simulations (B5) and observations increases to 0.7 (Fig. 4b), suggesting that accurately identifying the area of urban green areas not only

Table 4 Comparison of estimated BVOC emissions from urban green spaces in Beijing (unit: Gg)

References	Year	LAI	PFT	Isoprene	Monoterpenes	Sesquiterpenes	Total BVOCs
Ghirardo *et al.*[61]	2005	—	Tree inventory of 2005	2.62	0.38	0.34	4.82
Ghirardo *et al.*[61]	2010	—	Tree inventory of 2010	5.26	0.85	0.88	10.31
Ren *et al.*[26]	2015	The 2nd–7th national forest resource inventory	Field survey and the 8th national forest resource inventory	3.70	0.75	0.03	5.00
Li *et al.*[60]	2019	MOD15	FROM-GLC10	5.10	1.40	0.10	7.40
Li *et al.*[60]	2019	Calculated based on Sentinel-2 data	FROM-GLC10	4.25	1.20	0.08	6.24
This study	2017	GLASS	FROM-GLC10	4.94	0.45	0.09	8.43
This study	2017	GLASS	FROM-GLC10-U	9.05	1.16	0.21	13.40

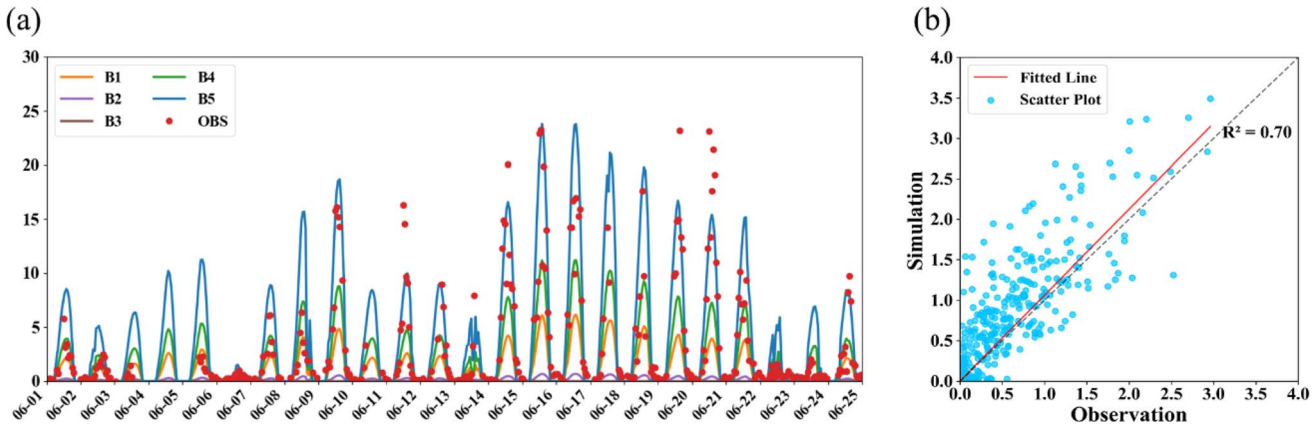

Fig. 4 Comparison between the observations and the simulations. (a) Time series of isoprene emissions with observations and different simulations in the IAP; the unit is nmol m^{-2} s^{-1}. (b) Evaluation of isoprene concentrations of B5 of observations and the simulations during June 1–25, 2017; R^2 is the correction coefficient; the unit is ppb.

improves the accuracy of the biogenic inventory but also better simulates isoprene concentrations in the atmosphere.

3.4 Contributions of BVOC emissions to O_3 and SOA

Fig. 5 presents the maximum daily averaged 8 h (MDA8) O_3 concentrations formed by BVOC emissions in the urban and rural areas of Beijing, which are calculated by the B4 case minus the B4-BJUNB case and the B4-BJUNB case minus the B4-BJNB case, respectively. The MDA8 O_3 is mainly concentrated in Chaoyang and Haidian districts, consistent with the description provided by Li *et al.*[60] High concentrations of MDA8 O_3 in Beijing urban areas typically exceed 5 ppb with the maximum value of 8 ppb due to the combined effect of urban green spaces and meteorological conditions. The higher temperature due to urban heat islands with lower humidity, as shown in Fig. S4,† makes urban areas hotter and drier, leading to more BVOC emissions and increasing ozone production.[10] Meanwhile, the urban area is full of anthropogenic emissions is the VOC-limited regime, where VOC is limited, but NO_x emissions are already high, so increased BVOC emissions greatly impact O_3 formation.[62] Fig. 5b indicates that in B5, the contribution of urban BVOCs to the MDA8 O_3 in Beijing is higher than in B4. The difference in biogenic ozone concentration between B5 and B4 in urban areas of Beijing exceeds 1.2 ppb. This increase is primarily due to the updated urban green spaces in B5, which

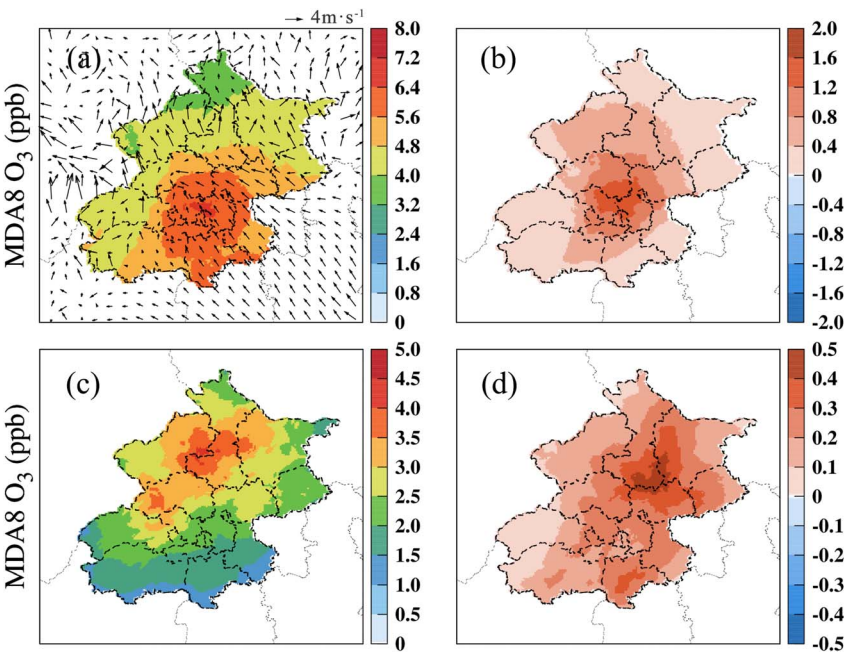

Fig. 5 The contributions of BVOC emissions to MDA8 O_3 concentrations from (a) urban green spaces and (c) rural vegetations in Beijing. The differences in contributions to MDA8 O_3 formed by (b) urban green spaces and (d) rural vegetations between the B5 case and the B4 case (B5–B4); the unit is ppb.

led to an approximately 40% increase in BVOC emissions. As a result, the O_3 concentration in urban areas increased by an average of 14.3%.

In addition to O_3 formed by urban BVOC emissions, Fig. 5c highlights the contribution of rural BVOC emissions to MDA8 O_3 concentrations in Beijing. The highest MDA8 O_3 concentrations, approximately 4 ppb, are observed in the northwest of Beijing, a region located downwind of the urban core, as illustrated by the wind direction in Fig. 5a. This downwind transport effect suggests that urban ozone precursors are carried to surrounding rural areas, elevating O_3 concentrations even where local emissions are relatively low. Comparing urban and rural areas, BVOC emissions are substantially higher in rural regions due to dense vegetation coverage, as shown in Fig. 3. However, the contribution of these rural BVOC emissions to O_3 concentrations is limited; this lower impact is largely due to the scarcity of NO_x in rural areas.[63] The contribution of urban vegetation to ozone in rural areas is close to that of the countryside itself, while the contribution of rural vegetation to ozone in urban areas is only about 1/4 that of the urban. Fig. 5d indicates the difference between the contribution from rural BVOC emissions to MDA8 O_3 concentrations in B5 and B4. The BVOC emissions in B5 contribute more MDA8 O_3 concentrations than in B4, with the differences primarily concentrated north of Beijing. However, this difference is slight, within 0.5 ppb, due to the relatively small variation in BVOC emissions in the rural areas of Beijing.

Fig. S3† presents the regional SOA concentrations formed by BVOC emissions (BSOA), including the contribution of BSOA concentrations from both inside and outside Beijing. The simulated BSOA concentrations are higher in northwestern Beijing, where the contributions exceed 5.6 μg m^{-3}, and lower in southeastern Beijing. The spatial distribution of BSOA in Beijing shows an increasing trend from southeast to northwest. This phenomenon is likely due to the higher density of vegetation in the northwest, which produces more BVOC emissions. Meanwhile, anthropogenic emissions from the urban core of Beijing are transported to the northwest by the summer monsoon (Fig. S4†), interacting with biogenic emissions and increasing oxidants, thereby enhancing BSOA formation in northwestern Beijing. Fig. S3b† shows the fractional contribution of BVOC emissions to SOA from the vegetation out of the Beijing areas, which usually contributes more than 25%. In the high vegetation density areas, the contribution rate to BSOA concentrations of regional transportation exceeds 35% and even reaches 40%, while in the southeastern part of Beijing, which is a flat terrain with highly distributed crops, the regional transportation contributes less than 30%.

To investigate the impact of urban BVOC emissions on the SOA, the spatial distribution of BSOA concentrations formed from urban green spaces in Beijing is shown in Fig. 6a. The mean concentrations of BSOA during the simulation period are 1.44 μg m^{-3} in the urban area. High BSOA concentrations are observed in central and southeastern Beijing, particularly in the core urban areas such as Dongcheng, Xicheng, and Haidian districts, with levels exceeding 1.8 μg m^{-3}. High temperatures in the urban areas have an enhanced effect on BSOA by promoting BVOC emissions.[10] According to studies on the BSOA compositions, the mean concentrations of isoprene-derived SOA (ISOA), monoterpene-derived SOA (MSOA), and sesquiterpene-derived SOA (SSOA) in urban area of Beijing are 0.64 μg m^{-3}, 0.29 μg m^{-3}, and 0.13 μg m^{-3}. The ISOA

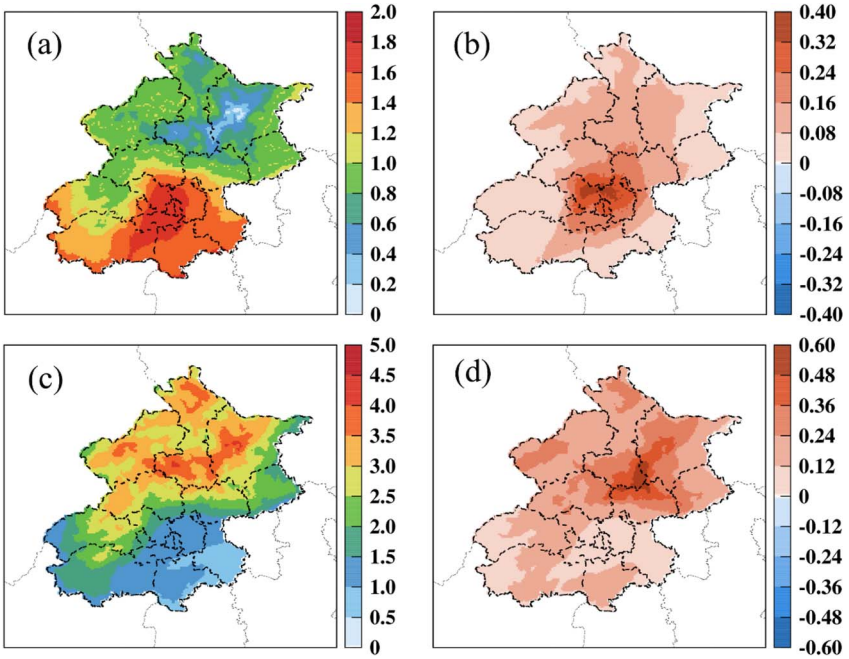

Fig. 6 (a) The contributions to SOA concentrations formed by BVOC emissions (BSOA) from urban green spaces and (b) the difference between the B5 case and the B4 case (B5–B4). (c) The contributions to BSOA concentrations from rural vegetation and (d) the difference between the B5 case and the B4 case; the unit is μg m^{-3}.

concentrations account for approximately 46% of BSOA from urban green spaces. This great contribution is attributed to the high density of broadleaf trees in urban areas with high isoprene emission rates (Fig. S5†). MSOA concentrations are lower compared to ISOA possibly due to the mediation of SO_2 and NO_x emitted by anthropogenic sources.[64]

Fig. 6b shows the difference in BSOA concentrations between the B5 case and the B4 case after updating the information on the urban green space in Beijing. The average difference in BSOA concentrations in urban areas reached 0.18 μg m^{-3} (10.6%), with the relative changes in ISOA, MSOA, and SSOA being 14.3%, 17.7%, and 32.6%, respectively. In the core urban areas of Beijing, such as Chaoyang and Haidian districts, peak differences in BSOA concentrations coincide with the distribution of high BVOC emissions. The average difference in BSOA concentrations in Chaoyang and Haidian districts is consistent, at 0.27 μg m^{-3}, with ISOA, MSOA, and SSOA contributing 45.8%, 24.3%, and 19.2%, respectively.

In addition to BSOA formed from the urban green spaces, the vegetation distributed in rural areas of Beijing also contributed significantly to the formation of SOA, as shown in Fig. 6c and d. In urban areas, BSOA concentrations are generally lower, reaching up to about 2.0 μg m^{-3} (Fig. 6a), whereas rural areas, particularly the northwest region such as Huairou district, exhibit peak BSOA concentrations reaching 4.8 μg m^{-3}. This urban–rural disparity is partly due to the higher BVOC emissions from rural vegetation (see Fig. 3), enhancing BSOA formation in these regions. The contribution of rural vegetation to SOA concentration in urban areas is 1.2 times that of urban green spaces, which indicates that rural vegetation contributes more to SOA concentration in Beijing than urban green spaces. This is primarily due to the large increase in oxidants (OH and O_3) facilitated by urban NO_x emissions.[65] Without the urban NO_x, the background NO_x emissions are mainly from soil microbial processes, which are much lower. Consequently, there is less production of OH and O_3, which leads to a reduced formation of BVOCs and SOA. Moreover, isoprene can be oxidized to form SOA *via* the isoprene epoxydiol pathway when the NO_x levels are low, which is higher than the SOA concentrations formed *via* the hydroxymethyl-α-lactone or 2-methyloxirane-2-carboxylic acid pathway when NO_x levels are high.[10]

4 Conclusions

In this study, we developed a new BVOC emission inventory with 1 km resolution by updating the spatial distribution and area of urban vegetation in Beijing, which were in turn compared with widely used BVOC emission inventories to assess its accuracy. Besides, the effects of BVOC emissions from urban green spaces on surface O_3 and SOA concentrations were also determined. The FROM-GLC10 dataset, the MCD12Q1 dataset, the CGLS dataset and the C3S dataset were used as land cover data input into MEGAN to generate BVOC emission inventories, which has differences in vegetation distributions and density in the urban area of Beijing. In the MCD12Q1 dataset, the coverage of urban green spaces is relatively lower than in other datasets. Although the urban green spaces of Beijing exceed 30% in the FROM-GLC10 dataset, it is still lower than the official data. The FROM-GLC10-U dataset updates the distribution and density of vegetation in Beijing, which is closer to the official data than the abovementioned land cover dataset. According to model simulation, the accuracy of the simulated isoprene emissions and concentrations in urban areas improved significantly after updating the urban green space.

High concentrations of MDA8 O_3 in Beijing urban areas typically exceed 5 ppb with the maximum of 8 ppb due to the combined effect of urban green spaces and meteorological conditions. In the rural area, the highest MDA8 O_3 concentrations (~4 ppb) formed by BVOCs are observed northwest of Beijing, attributed to its position downwind of the urban core. Although BVOC emissions are higher in rural areas than urban areas, their contribution to O_3 concentrations is lower in rural regions. In addition to biogenic O_3, SOA is another important sink of BVOCs. The mean concentrations of BSOA are 1.44 μg m^{-3} in the urban area, while the rural vegetation contributed more significantly to the SOA concentrations in the Beijing area, 1.2 times higher than that of urban green spaces.

Although high-resolution land cover datasets have improved the study of BVOC emissions, they still underestimate the distribution and density of vegetation in urban areas. The methodology used in this study helps to improve information on urban green spaces and is applicable to other areas. Thus, future work will use this method to construct a BVOC emission inventory of urban areas across China and determine the impacts on the urban atmospheric chemistry in China. However, the accuracy of the BVOC emission inventory could not be assessed due to the limitations of observations in BVOC components. Therefore, building up the observation database for BVOC components with field measurements is necessary.

Data availability

The CMAQ model code is available *via* the United States Environmental Protection Agency at **https://doi.org/10.5281/zenodo.1079898**, and the WRF model code is available on the WRF user page at **https://www2.mmm.ucar.edu/wrf/users/download/get_sources.html**. The observed isoprene data are available at the CEDA archive at **https://catalogue.ceda.ac.uk/uuid/9e11d5cb819a45068921db5ae296fb57**.

Conflicts of interest

The authors declare that they have no conflict of interest.

Acknowledgements

This work was supported by the National Natural Science Foundation of China (42077194/42377098/42375178) and the National Key Research and Development Program of China (2022YFC3703004/2022YFE0136200).

References

1 A. Goldstein and I. Galbally, Known and Unexplored Organic Constituents in the Earth's Atmosphere, *Environ. Sci. Technol.*, 2007, **41**, 1514–1521.
2 F. Fehsenfeld, J. Calvert, R. Fall, P. Goldan, A. B. Guenther, C. N. Hewitt, B. Lamb, S. Liu, M. Trainer, H. Westberg and P. Zimmerman, Emissions of volatile organic compounds from vegetation and the implications for atmospheric chemistry, *Global Biogeochem. Cycles*, 1992, **6**, 389–430.
3 A. Guenther, C. N. Hewitt, D. Erickson, R. Fall, C. Geron, T. Graedel, P. Harley, L. Klinger, M. Lerdau, W. A. McKay, T. Pierce, B. Scholes, R. Steinbrecher, R. Tallamraju, J. Taylor and P. Zimmerman, A global model of natural volatile organic compound emissions, *J. Geophys. Res.:Atmos.*, 1995, **100**, 8873–8892.
4 J. D. Fuentes, M. Lerdau, R. Atkinson, D. Baldocchi, J. W. Bottenheim, P. Ciccioli, B. Lamb, C. Geron, L. Gu, A. Guenther, T. D. Sharkey and W. Stockwell, Biogenic Hydrocarbons in the Atmospheric Boundary Layer, *Bull. Am. Meteorol. Soc.*, 2000, **81**, 1537–1576.
5 M. Mahilang, M. K. Deb and S. Pervez, Biogenic secondary organic aerosols: a review on formation mechanism, analytical challenges and environmental impacts, *Chemosphere*, 2021, **262**, 127771.
6 A. Poupkou, T. Giannaros, K. Markakis, I. Kioutsioukis, G. Curci, D. Melas and C. Zerefos, A Model for European Biogenic Volatile Organic Compound Emissions: Software Development and First Validation, *Environmental Modelling & Software*, 2010, **25**, 1845–1856.
7 A. Guenther, T. Karl, P. Harley, C. Wiedinmyer, P. I. Palmer and C. Geron, Estimates of global terrestrial isoprene emissions using MEGAN (Model of Emissions of Gases and Aerosols from Nature), *Atmos. Chem. Phys.*, 2006, **6**, 3181–3210.
8 A. Guenther, B. Baugh, G. Brasseur, J. Greenberg, P. Harley, L. Klinger, D. Serça and L. Vierling, Isoprene emission estimates and uncertainties for the central African EXPRESSO study domain, *J. Geophys. Res.:Atmos.*, 1999, **104**, 30625–30639.
9 W. J. F. Acton, Z. Huang, B. Davison, W. S. Drysdale, P. Fu, M. Hollaway, B. Langford, J. Lee, Y. Liu, S. Metzger, N. Mullinger, E. Nemitz, C. E. Reeves, F. A. Squires, A. R. Vaughan, X. Wang, Z. Wang, O. Wild, Q. Zhang, Y. Zhang and C. N. Hewitt, Surface–atmosphere fluxes of volatile organic compounds in Beijing, *Atmos. Chem. Phys.*, 2020, **20**, 15101–15125.
10 Y. Gao, M. Ma, F. Yan, H. Su, S. Wang, H. Liao, B. Zhao, X. Wang, Y. Sun, J. R. Hopkins, Q. Chen, P. Fu, A. C. Lewis, Q. Qiu, X. Yao and H. Gao, Impacts of biogenic emissions from urban landscapes on summer ozone and secondary organic aerosol formation in megacities, *Sci. Total Environ.*, 2022, **814**, 152654.
11 D. Y. C. Leung, P. Wong, B. K. H. Cheung and A. Guenther, Improved land cover and emission factors for modeling biogenic volatile organic compounds emissions from Hong Kong, *Atmos. Environ.*, 2010, **44**, 1456–1468.
12 D. C. Oderbolz, S. Aksoyoglu, J. Keller, I. Barmpadimos, R. Steinbrecher, C. A. Skjøth, C. Plaß-Dülmer and A. S. H. Prévôt, A comprehensive emission inventory of biogenic volatile organic compounds in Europe: improved seasonality and land-cover, *Atmos. Chem. Phys.*, 2013, **13**, 1689–1712.
13 A. B. Guenther, X. Jiang, C. L. Heald, T. Sakulyanontvittaya, T. Duhl, L. K. Emmons and X. Wang, The Model of Emissions of Gases and Aerosols from Nature version 2.1 (MEGAN2.1): an extended and updated framework for modeling biogenic emissions, *Geosci. Model Dev.*, 2012, **5**, 1471–1492.
14 H. Wang, Q. Wu, H. Liu, Y. Wang, H. Cheng, R. Wang, L. Wang, H. Xiao and X. Yang, Sensitivity of biogenic volatile organic compound emissions to leaf area index and land cover in Beijing, *Atmos. Chem. Phys.*, 2018, **18**, 9583–9596.
15 J. Ma, S. Zhu, S. Wang, P. Wang, J. Chen and H. Zhang, Impacts of land cover changes on biogenic emission and its contribution to ozone and secondary organic aerosol in China, *Atmos. Chem. Phys.*, 2023, **23**, 4311–4325.
16 M. Ma, Y. Gao, A. Ding, H. Su, H. Liao, S. Wang, X. Wang, B. Zhao, S. Zhang, P. Fu, A. B. Guenther, M. Wang, S. Li, B. Chu, X. Yao and H. Gao, Development and Assessment of a High-Resolution Biogenic Emission Inventory from Urban Green Spaces in China, *Environ. Sci. Technol.*, 2022, **56**, 175–184.
17 T. S. Eisenman, G. Churkina, S. P. Jariwala, P. Kumar, G. S. Lovasi, D. E. Pataki, K. R. Weinberger and T. H. Whitlow, Urban trees, air quality, and asthma: an interdisciplinary review, *Landscape and Urban Planning*, 2019, **187**, 47–59.
18 C. Calfapietra, S. Fares, F. Manes, A. Morani, G. Sgrigna and F. Loreto, Role of Biogenic Volatile Organic Compounds (BVOC) emitted by urban trees on ozone concentration in cities: a review, *Environ. Pollut.*, 2013, **183**, 71–80.
19 S. Gu, A. Guenther and C. Faiola, Effects of Anthropogenic and Biogenic Volatile Organic Compounds on Los Angeles Air Quality, *Environ. Sci. Technol.*, 2021, **55**, 12191–12201.
20 W. P. L. Carter, Development of Ozone Reactivity Scales for Volatile Organic Compounds, *Air Waste*, 1994, **44**, 881–899.
21 M. Ma, Y. Gao, Y. Wang, S. Zhang, L. R. Leung, C. Liu, S. Wang, B. Zhao, X. Chang, H. Su, T. Zhang, L. Sheng, X. Yao and H. Gao, Substantial ozone enhancement over the North China Plain from increased biogenic emissions due to heat waves and land cover in summer 2017, *Atmos. Chem. Phys.*, 2019, **19**, 12195–12207.
22 X. Ding, Q.-F. He, R.-Q. Shen, Q.-Q. Yu and X.-M. Wang, Spatial distributions of secondary organic aerosols from isoprene, monoterpenes, β-caryophyllene, and aromatics over China during summer, *J. Geophys. Res.:Atmos.*, 2014, **119**(11), 877–811, 891.
23 W. Kuang, Spatio-temporal patterns of intra-urban land use change in Beijing, China between 1984 and 2008, *Chinese Geographical Science*, 2012, **22**, 210–220.

24 C. N. B. o. S. (NBSC), *China Statistical Yearbook*, China Statistics Press, Beijing, 2022.
25 M. o. H. a. U.-R. D. (PRC), *Yearbook of Urban and Rural Construction Statistics*, 2023, https://www.mohurd.gov.cn/gongkai/fdzdgknr/sjfb/tjxx/jstjnj/index_2.html.
26 Y. Ren, Z. Qu, Y. Du, R. Xu, D. Ma, G. Yang, Y. Shi, X. Fan, A. Tani, P. Guo, Y. Ge and J. Chang, Air quality and health effects of biogenic volatile organic compounds emissions from urban green spaces and the mitigation strategies, *Environ. Pollut.*, 2017, **230**, 849–861.
27 T. Wang, L. Xue, P. Brimblecombe, Y. F. Lam, L. Li and L. Zhang, Ozone pollution in China: a review of concentrations, meteorological influences, chemical precursors, and effects, *Sci. Total Environ.*, 2017, **575**, 1582–1596.
28 Z. Tan, X. Ma, K. Lu, M. Jiang, Q. Zou, H. Wang, L. Zeng and Y. Zhang, Direct evidence of local photochemical production driven ozone episode in Beijing: a case study, *Sci. Total Environ.*, 2021, **800**, 148868.
29 X. Lu, L. Zhang, Y. Chen, M. Zhou, B. Zheng, K. Li, Y. Liu, J. Lin, T. M. Fu and Q. Zhang, Exploring 2016–2017 surface ozone pollution over China: source contributions and meteorological influences, *Atmos. Chem. Phys.*, 2019, **19**, 8339–8361.
30 K. Li, D. J. Jacob, L. Shen, X. Lu, I. De Smedt and H. Liao, Increases in surface ozone pollution in China from 2013 to 2019: anthropogenic and meteorological influences, *Atmos. Chem. Phys.*, 2020, **20**, 11423–11433.
31 J. Sun, Z. Shen, R. Wang, G. Li, Y. Zhang, B. Zhang, K. He, Z. Tang, H. Xu, L. Qu, S. Sai Hang Ho, S. Liu and J. Cao, A comprehensive study on ozone pollution in a megacity in North China Plain during summertime: observations, source attributions and ozone sensitivity, *Environ. Int.*, 2021, **146**, 106279.
32 P. Gong, H. Liu, M. Zhang, C. Li, J. Wang, H. Huang, N. Clinton, L. Ji, W. Li, Y. Bai, B. Chen, B. Xu, Z. Zhu, C. Yuan, H. Ping Suen, J. Guo, N. Xu, W. Li, Y. Zhao, J. Yang, C. Yu, X. Wang, H. Fu, L. Yu, I. Dronova, F. Hui, X. Cheng, X. Shi, F. Xiao, Q. Liu and L. Song, Stable classification with limited sample: transferring a 30-m resolution sample set collected in 2015 to mapping 10-m resolution global land cover in 2017, *Sci. Bull.*, 2019, **64**, 370–373.
33 Z. Xiao, S. Liang, J. Wang, P. Chen, X. Yin, L. Zhang and J. Song, Use of General Regression Neural Networks for Generating the GLASS Leaf Area Index Product from Time-Series MODIS Surface Reflectance, *IEEE Transactions on Geoscience and Remote Sensing*, 2014, **52**, 209–223.
34 Z. Xiao, S. Liang, J. Wang, Y. Xiang, X. Zhao and J. Song, Long-Time-Series Global Land Surface Satellite Leaf Area Index Product Derived from MODIS and AVHRR Surface Reflectance, *IEEE Transactions on Geoscience and Remote Sensing*, 2016, **54**, 5301–5318.
35 X. Yang, X. Zhiqiang, L. Shunlin, W. Jindi and S. Jinling, Validation of Global LAnd Surface Satellite (GLASS) leaf area index product, *J. Remote Sens.*, 2014, **18**, 573–596.
36 C3S, *Land cover classification gridded maps from 1992 to present derived from satellite observation*, Copernicus Climate Change Service (C3S) Climate Data Store (CDS), 2019, DOI: 10.24381/cds.006f2c9a.
37 M. Friedl and D. Sulla-Menashe, *MCD12Q1 MODIS/Terra+Aqua Land Cover Type Yearly L3 Global 500m SIN Grid V006*, NASA EOSDIS Land Processes DAAC, 2019, DOI: 10.5067/MODIS/MCD12Q1.006.
38 M. Buchhorn, B. Smets, L. Bertels, B. DeRoo, M. Lesiv, N.-E. Tsendbazar, M. Herold and S. Fritz, *Copernicus Global Land Service: Land Cover 100m: Collection 3: Epoch 2019: Globe (V3.0.1)*, Zenodo, 2020, DOI: 10.5281/zenodo.3939050.
39 Y. Xu, L. Yu, D. Feng, D. Peng, C. Li, X. Huang, H. Lu and P. Gong, Comparisons of three recent moderate resolution African land cover datasets: CGLS-LC100, ESA-S2-LC20, and FROM-GLC-Africa30, *International Journal of Remote Sensing*, 2019, **40**, 6185–6202.
40 SFA, *Report of China Forest Resources (2014-2018)*, China Forestry Press, 2019.
41 D. J. Bryant, W. J. Dixon, J. R. Hopkins, R. E. Dunmore, K. L. Pereira, M. Shaw, F. A. Squires, T. J. Bannan, A. Mehra, S. D. Worrall, A. Bacak, H. Coe, C. J. Percival, L. K. Whalley, D. E. Heard, E. J. Slater, B. Ouyang, T. Cui, J. D. Surratt, D. Liu, Z. Shi, R. Harrison, Y. Sun, W. Xu, A. C. Lewis, J. D. Lee, A. R. Rickard and J. F. Hamilton, Strong anthropogenic control of secondary organic aerosol formation from isoprene in Beijing, *Atmos. Chem. Phys.*, 2020, **20**, 7531–7552.
42 K. M. Foley, S. J. Roselle, K. W. Appel, P. V. Bhave, J. E. Pleim, T. L. Otte, R. Mathur, G. Sarwar, J. O. Young, R. C. Gilliam, C. G. Nolte, J. T. Kelly, A. B. Gilliland and J. O. Bash, Incremental testing of the Community Multiscale Air Quality (CMAQ) modeling system version 4.7, *Geosci. Model Dev.*, 2010, **3**, 205–226.
43 Q. Ying, J. Li and S. H. Kota, Significant Contributions of Isoprene to Summertime Secondary Organic Aerosol in Eastern United States, *Environ. Sci. Technol.*, 2015, **49**, 7834–7842.
44 G. L. Gipson and J. O. Young, *Gas-Phrase Chemistry*, EPA, 1999.
45 Y.-H. Lin, H. Zhang, H. O. T. Pye, Z. Zhang, W. J. Marth, S. Park, M. Arashiro, T. Cui, S. H. Budisulistiorini, K. G. Sexton, W. Vizuete, Y. Xie, D. J. Luecken, I. R. Piletic, E. O. Edney, L. J. Bartolotti, A. Gold and J. D. Surratt, Epoxide as a precursor to secondary organic aerosol formation from isoprene photooxidation in the presence of nitrogen oxides, *Proc. Natl. Acad. Sci. U. S. A.*, 2013, **110**, 6718–6723.
46 Y. Xie, F. Paulot, W. P. L. Carter, C. G. Nolte, D. J. Luecken, W. T. Hutzell, P. O. Wennberg, R. C. Cohen and R. W. Pinder, Understanding the impact of recent advances in isoprene photooxidation on simulations of regional air quality, *Atmos. Chem. Phys.*, 2013, **13**, 8439–8455.
47 F. Paulot, J. D. Crounse, H. G. Kjaergaard, A. Kürten, J. M. St. Clair, J. H. Seinfeld and P. O. Wennberg, Unexpected Epoxide Formation in the Gas-Phase Photooxidation of Isoprene, *Science*, 2009, **325**, 730–733.

48 C. Fountoukis, D. Koraj, H. A. C. Denier van der Gon, P. E. Charalampidis, C. Pilinis and S. N. Pandis, Impact of grid resolution on the predicted fine PM by a regional 3-D chemical transport model, *Atmos. Environ.*, 2013, **68**, 24–32.

49 C.-M. Gan, C. Hogrefe, R. Mathur, J. Pleim, J. Xing, D. Wong, R. Gilliam, G. Pouliot and C. Wei, Assessment of the effects of horizontal grid resolution on long-term air quality trends using coupled WRF-CMAQ simulations, *Atmos. Environ.*, 2016, **132**, 207–216.

50 A. Torres-Vazquez, J. Pleim, R. Gilliam and G. Pouliot, Performance Evaluation of the Meteorology and Air Quality Conditions from Multiscale WRF-CMAQ Simulations for the Long Island Sound Tropospheric Ozone Study (LISTOS), *J. Geophys. Res.:Atmos.*, 2022, **127**, e2021JD035890.

51 P. Wang, K. Chen, S. Zhu, P. Wang and H. Zhang, Severe air pollution events not avoided by reduced anthropogenic activities during COVID-19 outbreak, *Resour., Conserv. Recycl.*, 2020, **158**, 104814.

52 S. Zhu, J. Poetzscher, J. Shen, S. Wang, P. Wang and H. Zhang, Comprehensive Insights into O_3 Changes during the COVID-19 from O_3 Formation Regime and Atmospheric Oxidation Capacity, *Geophys. Res. Lett.*, 2021, **48**, e2021GL093668.

53 B. Zheng, D. Tong, M. Li, F. Liu, C. Hong, G. Geng, H. Li, X. Li, L. Peng, J. Qi, L. Yan, Y. Zhang, H. Zhao, Y. Zheng, K. He and Q. Zhang, Trends in China's anthropogenic emissions since 2010 as the consequence of clean air actions, *Atmos. Chem. Phys.*, 2018, **18**, 14095–14111.

54 S. Zhu, J. Ma, S. Wang, S. Sun, P. Wang and H. Zhang, Shifts of Formation Regimes and Increases of Atmospheric Oxidation Led to Ozone Increase in North China Plain and Yangtze River Delta From 2016 to 2019, *J. Geophys. Res.:Atmos.*, 2023, **128**, e2022JD038373.

55 S. Zhang, Z. Zhang, Y. Li, X. Du, L. Qu, W. Tang, J. Xu and F. Meng, Formation processes and source contributions of ground-level ozone in urban and suburban Beijing using the WRF-CMAQ modelling system, *J. Environ. Sci.*, 2023, **127**, 753–766.

56 H. Matsui, M. Koike, Y. Kondo, N. Takegawa, K. Kita, Y. Miyazaki, M. Hu, S. Y. Chang, D. R. Blake, J. D. Fast, R. A. Zaveri, D. G. Streets, Q. Zhang and T. Zhu, Spatial and temporal variations of aerosols around Beijing in Summer 2006: model evaluation and source apportionment, *J. Geophys. Res.:Atmos.*, 2009, **114**, D00G13.

57 U. S. EPA, *Guidance on the Use of Models and Other Analyses in Attainment Demonstrations for the 8-Hour Ozone NAAQS*, 2005, EPA-454/R-05-002.

58 P. Wang, J. Shen, M. Xia, S. Sun, Y. Zhang, H. Zhang and X. Wang, Unexpected enhancement of ozone exposure and health risks during National Day in China, *Atmos. Chem. Phys.*, 2021, **21**, 10347–10356.

59 R. Seco, J. Peñuelas, I. Filella, J. Llusià, R. Molowny-Horas, S. Schallhart, A. Metzger, M. Müller and A. Hansel, Contrasting winter and summer VOC mixing ratios at a forest site in the Western Mediterranean Basin: the effect of local biogenic emissions, *Atmos. Chem. Phys.*, 2011, **11**, 13161–13179.

60 X. Li, W. Chen, H. Zhang, T. Xue, Y. Zhong, M. Qi, X. Shen and Z. Yao, Emissions of biogenic volatile organic compounds from urban green spaces in the six core districts of Beijing based on a new satellite dataset, *Environ. Pollut.*, 2022, **308**, 119672.

61 A. Ghirardo, J. Xie, X. Zheng, Y. Wang, R. Grote, K. Block, J. Wildt, T. Mentel, A. Kiendler-Scharr, M. Hallquist, K. Butterbach-Bahl and J. P. Schnitzler, Urban stress-induced biogenic VOC emissions and SOA-forming potentials in Beijing, *Atmos. Chem. Phys.*, 2016, **16**, 2901–2920.

62 K. Wu, X. Yang, D. Chen, S. Gu, Y. Lu, Q. Jiang, K. Wang, Y. Ou, Y. Qian, P. Shao and S. Lu, Estimation of biogenic VOC emissions and their corresponding impact on ozone and secondary organic aerosol formation in China, *Atmos. Res.*, 2020, **231**, 104656.

63 A. C. Fitzky, H. Sandén, T. Karl, S. Fares, C. Calfapietra, R. Grote, A. Saunier and B. Rewald, The Interplay between Ozone and Urban Vegetation—BVOC Emissions, *Ozone Deposition, and Tree Ecophysiology*, 2019, **2**, 50.

64 L. Xu, H. Guo, C. M. Boyd, M. Klein, A. Bougiatioti, K. M. Cerully, J. R. Hite, G. Isaacman-VanWertz, N. M. Kreisberg, C. Knote, K. Olson, A. Koss, A. H. Goldstein, S. V. Hering, J. de Gouw, K. Baumann, S.-H. Lee, A. Nenes, R. J. Weber and N. L. Ng, Effects of anthropogenic emissions on aerosol formation from isoprene and monoterpenes in the southeastern United States, *Proc. Natl. Acad. Sci. U. S. A.*, 2015, **112**, 37–42.

65 M. Shrivastava, M. O. Andreae, P. Artaxo, H. M. J. Barbosa, L. K. Berg, J. Brito, J. Ching, R. C. Easter, J. Fan, J. D. Fast, Z. Feng, J. D. Fuentes, M. Glasius, A. H. Goldstein, E. G. Alves, H. Gomes, D. Gu, A. Guenther, S. H. Jathar, S. Kim, Y. Liu, S. Lou, S. T. Martin, V. F. McNeill, A. Medeiros, S. S. de Sá, J. E. Shilling, S. R. Springston, R. A. F. Souza, J. A. Thornton, G. Isaacman-VanWertz, L. D. Yee, R. Ynoue, R. A. Zaveri, A. Zelenyuk and C. Zhao, Urban pollution greatly enhances formation of natural aerosols over the Amazon rainforest, *Nat. Commun.*, 2019, **10**, 1046.